Liquid Crystals
Publication details, including instructions for authors and subscription information:
http://www.informaworld.com/smpp/title~content=t713926090

Kinetics of nanocolloids in the aligned domain of octylcyanobiphenyl and aerosil dispersion

Dipti Sharma[a]
[a] Department of Physics, Worcester Polytechnic Institute, Worcester, MA 01609

To cite this Article Sharma, Dipti(2008) 'Kinetics of nanocolloids in the aligned domain of octylcyanobiphenyl and aerosil dispersion', Liquid Crystals, 35: 10, 1215 — 1224
To link to this Article: DOI: 10.1080/02678290802509400
URL: http://dx.doi.org/10.1080/02678290802509400

Liquid Crystals,
Vol. 35, No. 10, October 2008, 1215–1224

Taylor & Francis
Taylor & Francis Group

Kinetics of nanocolloids in the aligned domain of octylcyanobiphenyl and aerosil dispersion

Dipti Sharma*

Department of Physics, Worcester Polytechnic Institute, Worcester, MA 01609, USA

(Received 8 May 2008; final form 26 September 2008)

In this study we explore the interesting kinetics of nanocolloids formed by the solvent dispersion method (SDM) in an aligned matrix of octylcyanobiphenyl (8CB) liquid crystals and aerosil nanoparticles. The presence of alignment changes the behaviour of the induced crystallisation (IC), and melting transition (*K*–Sm*A*) observed in the aligned nanocolloidal liquid crystal samples when compared with unaligned samples. Heating-rate-dependent experiments were performed for the aligned and unaligned samples at various heating ramp rates varied from 20 to 1 K min^{-1} using a calorimetric technique. In the aligned samples, the IC transition peak shifts towards higher temperature, whereas the melting transition peak shifts towards lower temperature. The IC peak shows an increase in enthalpy whereas the melting transition shows a decrease following an Arrhenius behaviour. The presence of alignment increases the activated kinetics of the system. This behaviour can be explained in terms of molecular interaction between aligned domains of nanocolloids in the 8CB matrix which makes the material stiffer.

Keywords: liquid crystal; Arrhenius theory; surface kinetics; calorimeter; magnetic effect on phase transitions

1. Introduction

The suspension of nanocolloids in the liquid crystal (LC) creates a random disorder on phase transitions of LC systems and has been an interesting area for researchers and scientists in understanding the interaction between LC molecules and aerosil nanoparticles (*1–5*). In the LC+aerosil systems, the quenched random disorder is created by a dispersed gel of aerosil nanoparticles and is varied by changing the density of aerosils in the dispersion. The aerosils used are silica spheres that can hydrogen bond together to form a fractal-like random gel. Studies have previously been carried out by various groups on such systems to study phase transitions (*1, 5, 6*). It would be interesting to study these types of systems under the effect of magnetic field to explore the change in the interaction between aerosil nanoparticles and LC molecules. A couple of studies report the effect of a magnetic field on the bulk LC systems using optical and rheological techniques (*7–11*). These studies focussed on smectic-*A* to nematic (Sm*A*–*N*) and nematic to isotropic (*N*–*I*) transitions. However, no literature has been found on crystallisation and melting transitions under the effect of a magnetic field. Moreover, no study reports the activated kinetics and thermodynamics of these transitions for aligned LC systems and seems to be absent from the literature. Hence, these types of studies are still open to be investigated. Therefore, we have undertaken a detailed calorimetric experiments to study thermodynamics of the induced crystallisation (IC) and melting transition of an aligned nanocolloidal octylcyanobiphenyl (8CB) LC system. Calorimetry technique has been using to study various research materials for decades (*5, 12–20*).

Here we report the effect of alignment on the activated kinetics of the IC and melting transition of a nanocolloidal 8CB system following Arrhenius theory. Heating scans were performed at four different heating ramp rates using differential scanning calorimetry (DSC). Three multiple densities of the aerosil nanoparticles in 8CB were studied to explore the effect of aerosil nanoparticles in bulk 8CB. Samples and calorimetry are described in Section 2. The results are shown in Section 3, with a discussion and conclusions given in Section 4.

2. Experimental section

2.1. *Formation of aligned nanocolloids*

The nanocolloidal samples were prepared by mixing aerosil nanoparticles in the bulk 8CB LC using the solvent dispersion method (SDM) (*5, 20–22*). The 8CB LC used in this work is a well-studied prototypical rod-like molecule, with a rigid biphenyl core at one end attached to an aliphatic tail and other to a polar cyano group. The aerosil consists of SiO_2 (silica) spheres coated with hydroxyl (–OH) groups exposed on the surface. The hydroxyl groups on the surface enable the spheres to hydrogen bond and

*Email: dr_dipti_sharma@yahoo.com

ISSN 0267-8292 print/ISSN 1366-5855 online

DOI: 10.1080/02678290802509400
http://www.informaworld.com

form a thixotropic (a property of certain gels to become fluid when mechanically disturbed (as by shaking or stirring) then resetting after a period of time), fractal gel in an organic medium such as 8CB. The hydrophilic nature of the aerosils allows the silica particles to weakly hydrogen bond to each other and form a gel in an organic solvent, however the basic free-floating aerosil unit typically consists of several of these spheres fused together during the manufacturing process (*4, 20*). Each 8CB and silica sample was created by mixing appropriate quantities of LC and aerosil together, then dissolving the resulting mixture in spectroscopic grade (low water content) acetone. The resulting solution was then dispersed using an ultrasonic bath for about an hour. As the acetone evaporates from the mixture, a fractal-like gel forms through diffusion-limited aggregation. Crystallisation of the LC host can severely disrupt the gel structure and so care was taken to prevent any formation of the solid phase of the LC during the experiments. The samples were subsequently dried under vacuum for more than 2 h at elevated temperature. This preparation method has been shown to produce uniform and reproducible dispersions (*4, 20*).

The bulk 8*CB* was obtained from Frinton Laboratories and aerosil nanoparticles were obtained from Degussa (Degussa Corp., Silica Division, Ridgefield Park, NJ, USA; technical data is given in the Degussa booklet Aerosila). The specific surface area of type-300 aerosil nanoparticle is $300\,m^2\,g^{-1}$ and the diameter of aerosil nanoparticles is roughly 7 nm whereas the length of 8CB molecules is 2 nm and the width is 0.5 nm. The molecular weight of bulk 8CB and aerosil nanoparticles (SiO_2) are $M_w = 291.44\,g\,mol^{-1}$ and $M_w = 60.08\,g\,mol^{-1}$, respectively. The density of the aerosil nanoparticles varied from 0 to $0.2\,g\,cm^{-3}$ in the bulk 8CB. The density of the aerosil nanoparticles in the bulk of 8CB was varied in three steps from 0 to $0.2\,g\,cm^{-3}$. The density of silica was 0.05, 0.10 and $0.20\,g\,cm^{-3}$. These samples were degassed for about an hour under a vacuum unit at room temperature 293 K and then used for magnetisation.

To obtain an aligned system, aerosil dispersed LC 8CB samples were exposed to the magnetic field. A magnet field of 0.5 T was used to create a magnetic field. First the unaligned samples (2 mg) were sealed in the aluminium pans and then they were heated until isotropic transition (318 K) and then they were placed immediately into the magnetic field. During the process of magnetisation, the sealed samples were kept in between a magnet of intensity 0.5 T where temperature of the sample varied in between smectic *A* and isotropic phases. The temperature range of this cycling was 300–318 K. The number of cycling was 10. After treating sample under magnetic field, a change in the transparency of the sample took place. Aligned sample changes into transparent color from the translucent whitish color. The change in the color of the aligned samples indicates changes in the alignment of the LC molecules and their domains. As the sample becomes magnetised, LC molecules form aligned domains and this alignment imposes a force on the aerosil nanoparticles covered with 8CB molecules and makes the nanocolloids aligned in the aligned domains of LCs. The aligned samples remain magnetised or transparent until they are heated to the isotropic phase. To understand the molecular alignment and interaction between LC molecules and aerosil nanoparticles, these aligned samples then underwent DSC for calorimetric measurements with the unaligned samples from the same batch as the aligned samples. Freshly aligned samples were used for each of the DSC experiments. Once the aligned samples were heated to the isotropic temperature range, they were not used again to prevent them from unalignment due to the heating. The calorimetric details for the experiments performed are as follows.

2.2. *Calorimetry*

To understand the thermodynamics of the aerosil dispersed 8CB system, we study the rate kinetics of the IC and melting transitions using DSC (model MDSC 2920, TA instruments). Three different densities of aerosil particles were studied in bulk 8CB: 0.05, 0.10 and $0.20\,g\,cm^{-3}$. First the sealed aligned samples were quenched at 243 K and then kept isothermal for 10 min. The aligned sample (2 mg of lowest density $0.05\,g\,cm^{-3}$) was heated from 243 to 333 K at a ramp rate of $20\,K\,min^{-1}$. The respective heat flow of the sample was recorded along with temperature change during heating scans. The thermograms showed an exothermic peak for IC and then a endothermic peak for the melting transition (*K*–Sm*A*) in the aerosil dispersed 8CB system. Two further endothermic peaks were also observed on heating scans at Sm*A*–*N* and *N*–*I* transitions. Here, we focus on IC and melting transitions only. Similar measurements were made at other heating scan rates of 10, 5, and $1\,K\,min^{-1}$ with the freshly aligned samples. Experimental and environmental conditions were kept identical for all runs. The above steps were repeated for other densities of aerosil nanoparticles (0.10 and $0.20\,g\,cm^{-3}$) using the same procedure. The equipment was well calibrated. All heating scans were

repeated several times using freshly aligned samples to ensure the accuracy of results.

Purity analysis for the bulk 8CB and its aerosil mixture performed experimentally. Transition temperatures of the pure 8CB as well as that used for the mixtures were compared with the highest reported values for isotropic to nematic (*I–N*) and for nematic to smectic A (*N*–Sm*A*) phases, and those were found to be consistent (e.g. for the bulk 8CB, T_{IN}=314.0 K and T_{SmAN}=307.0 K using an AC calorimetry technique).

3. Results

3.1. *Effect of the heating scan*

Heating an aligned nanocolloidal 8CB system brings an interesting change in the positions of the IC and melting transitions (*K*–Sm*A*). As the temperature increases from 243 to 333 K, the aerosil dispersed system shows an exothermic peak at 273.8 K (=0.8°C) as it moves from its solid state (*S*) to crystalline state (*K*) in the absence of alignment, as shown by the open symbols in Figure 1. It is an additional and interesting peak observed in the presence of aerosil particles in the system before melting. We already introduced this exothermic peak as IC in our recent publication (*5*). In an aligned system, this IC transition appears at 277.9 K (=4.9°C) at the same heating rate and shows a temperature shift in IC towards higher temperature by 4 K. As the heating scan continues further, a endothermic peak was observed for the melting transition at 294.3 K (=21.3°C) in the absence of alignment. Whereas the same melting peak appears in the aligned samples at 293.6 K (=20.6°C), this is a shift by around 0.7 K towards the lower temperature. The interesting thing is that both transitions show a temperature shift in opposite directions in the presence of alignment. In addition, in the aligned system, the IC peak becomes wider whereas the melting peak becomes narrower, and this shows changes in their associated enthalpy. The IC peak shows an increase in its enthalpy, shown in Figure 2, whereas the melting transition shows a decrease in its enthalpy for the aligned system, as shown in Figure 3.

3.2. *Effect of the heating rate*

A rate dependent study was also performed at different heating ramp rates of 20, 10, 5 and 1 K min^{-1} for all densities in the presence of alignment, as shown in Figure 4. As the ramp rate decreases, IC and melting transitions shift towards a lower temperature following Arrhenius behaviour, and the peak seems to be smaller and broader. To see a clear shift in each transition, the excess of the specific heat capacity can be plotted for transitions. The excess of the specific heat capacity of the system

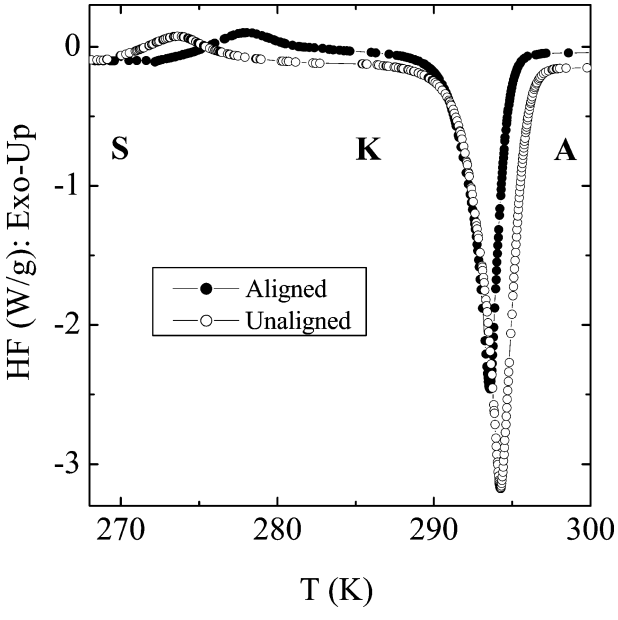

Figure 1. Heat flow versus temperature at 5 K min^{-1} heating ramp rate for a density of 0.05 g cm^{-3}. The regions *S*, *K* and *A* represents solid, crystalline and smectic A states of the system, respectively. Closed and open symbols represent aligned and unaligned systems, respectively.

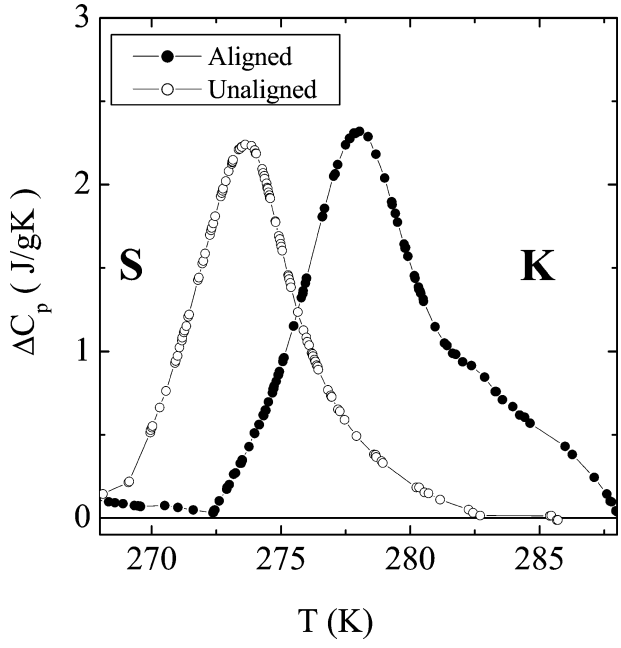

Figure 2. The excess of specific heat capacity (J g^{-1} K^{-1}) versus temperature (K) plot for the IC transition at 5 K min^{-1} for a density of 0.05 g cm^{-3}. Closed and open symbols represent aligned and unaligned systems, respectively.

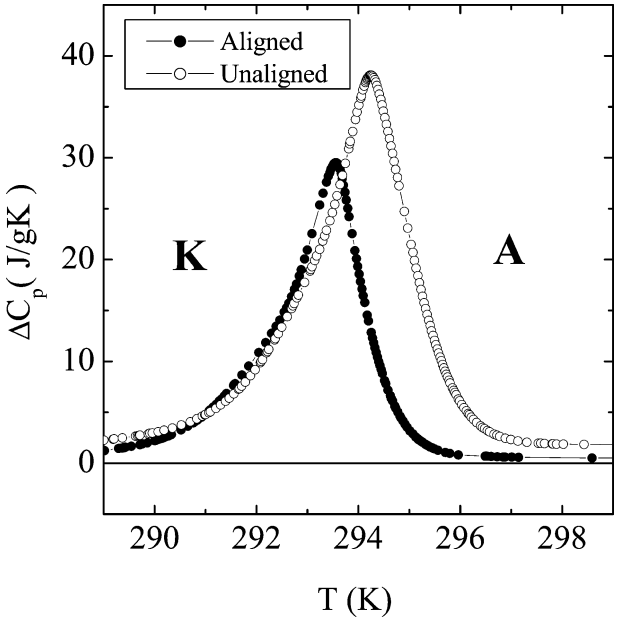

Figure 3. The excess of specific heat capacity ($J\,g^{-1}\,K^{-1}$) versus temperature (K) plot for the melting or *K*–Sm*A* transition at the same ramp rate for a density of $0.05\,g\,cm^{-3}$. Closed and open symbols represent aligned and unaligned systems, respectively.

can be obtained by subtracting from the specific heat C_p a linear background as

$$\Delta C_p = C_p - C_p(\text{background}), \qquad (1)$$

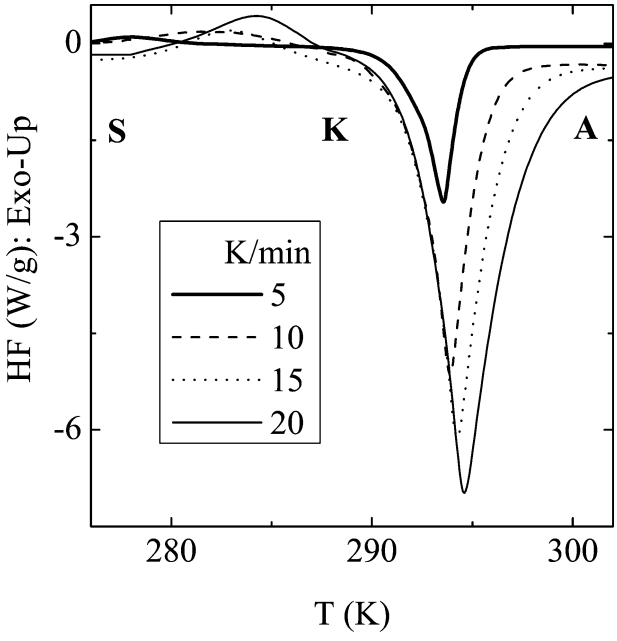

Figure 4. Effect of heating rate on alignment: heat flow ($W\,g^{-1}$) versus temperature (K) for $0.05\,g\,cm^{-3}$ density of aerosil for heating scan at different ramp rates from 20 to $5\,K\,min^{-1}$.

where C_p (background) is the baseline and C_p is the specific heat capacity of the sample. As the ramp rates decreases, the IC peak shifts towards lower temperature with an increased shifting rate in the presence of alignment, as shown in Figure 5. Figure 6 shows that the melting peak shifts with a smaller shifting rate towards a lower temperature with decreasing ramp rate in the presence of alignment. Both transitions follow Arrhenius behaviour. Activation energy can be calculated for each transition using the following Arrhenius rate-dependent theory.

According to Arrhenius theory, (*23–26*) the effective heating rate can be given by

$$\beta = \beta_0 \left(\exp\left(\frac{-\Delta E}{RT} \right) \right), \qquad (2)$$

where β ($K\,min^{-1}$) is the effective heating rate, β_0 ($K\,min^{-1}$) is a constant, ΔE ($J\,mol^{-1}$) is the activation energy, R ($J\,mol^{-1}\,K^{-1}$) is the universal gas constant

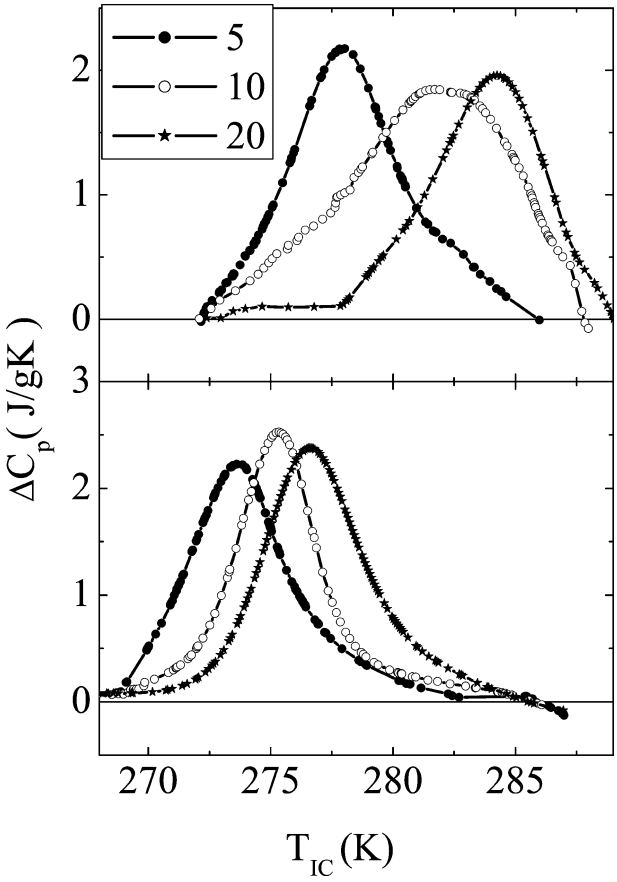

Figure 5. The excess of specific heat capacity ($J\,g^{-1}\,K^{-1}$) versus temperature (K) for the IC transition with varying ramp rates from 20 to $5\,K\,min^{-1}$ for a density of $0.05\,g\,cm^{-3}$. Upper section: aligned systems; lower section: unaligned systems.

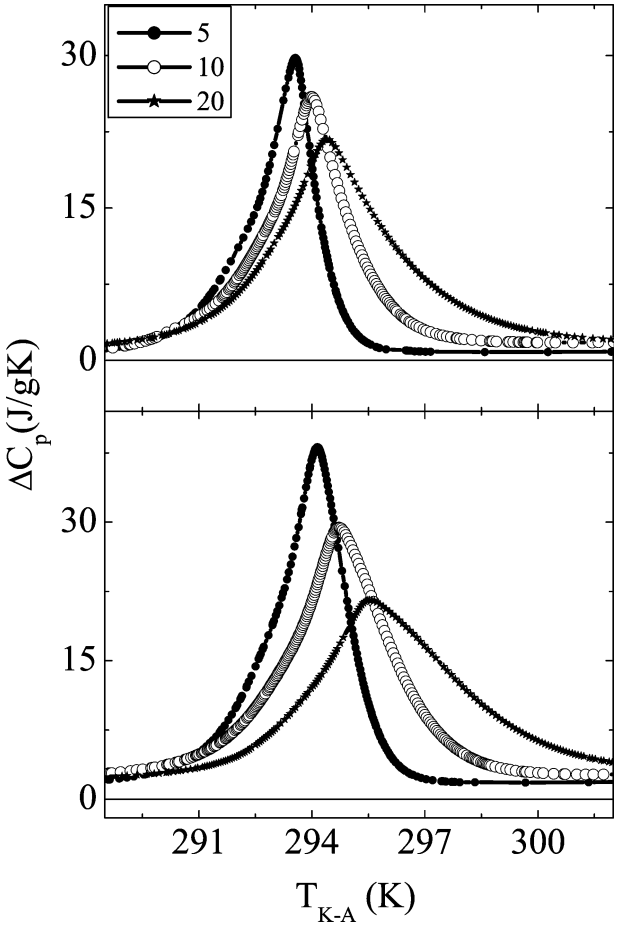

Figure 6. The excess of specific heat capacity ($J\,g^{-1}\,K^{-1}$) versus temperature (K) for the *K*–Sm*A* transition for the same ramp rates varying from 20 to 5 K min^{-1} for a density of 0.05 g cm^{-3}. Upper section: aligned systems; lower section: unaligned systems.

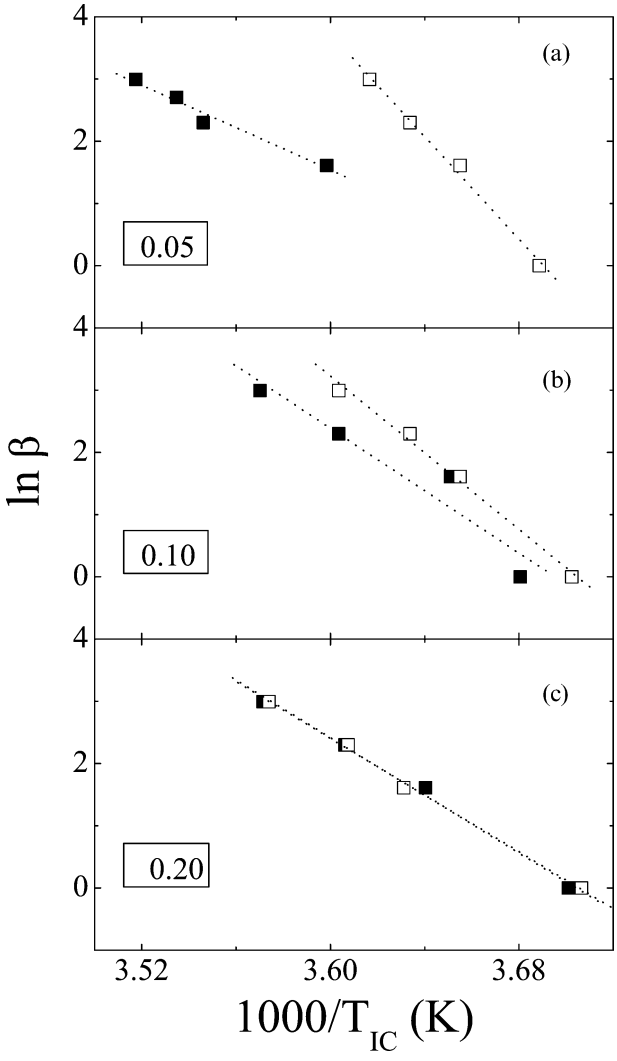

Figure 7. Arrhenius behaviour for the IC transition: lnβ (K min^{-1}) versus $1/T$ (K) for various densities: (A) 0.05 g cm^{-3}; (B) 0.10 g cm^{-3}; (C) 0.20 g cm^{-3}. Dotted lines are the fits to the data points. Closed and open symbols represent the aligned and unaligned systems, respectively.

and T (K) is the absolute temperature. This equation can also be written as

$$\ln \beta = \ln \beta_0 - \left(\frac{\Delta E}{RT}\right), \tag{3}$$

where ΔE is determined from the slope of the graph, which is plotted between lnβ and $1/T$.

Rate effects for IC and the melting transitions were also found for other densities of nanocolloids (0.10 to 0.20 g cm^{-3}) in the presence of alignment. For simplicity, these plots are not shown here but these results are considered in the data analysis. The activation energy of the aligned IC transition decreases for the lowest density of nanocolloids 0.05 g cm^{-3}, and then increases for 0.10 and remains smaller than the unaligned values, and then becomes almost equal to the value of unaligned system for the highest density of nanocolloids 0.20 g cm^{-3}, as shown in Figure 7. The activation energy for the aligned melting transition increases for 0.05, then decreases for 0.10, and then increases for 0.20 g cm^{-3} of nanocolloids when compared with the unaligned values, as shown in Figure 8. IC and melting transitions show the opposite behaviour for activation energy in the presence of alignment. The data for the activation energy of aligned and unaligned systems can be seen in Table 1.

3.3. *Effect on density variation of nanocolloids*

The clear effect of alignment on the density of nanocolloids in LCs were observed for IC and melting transitions. As aerosil density increases in the aligned system, the IC transition becomes wider and shows multiple peaks, as shown in Figure 9. It

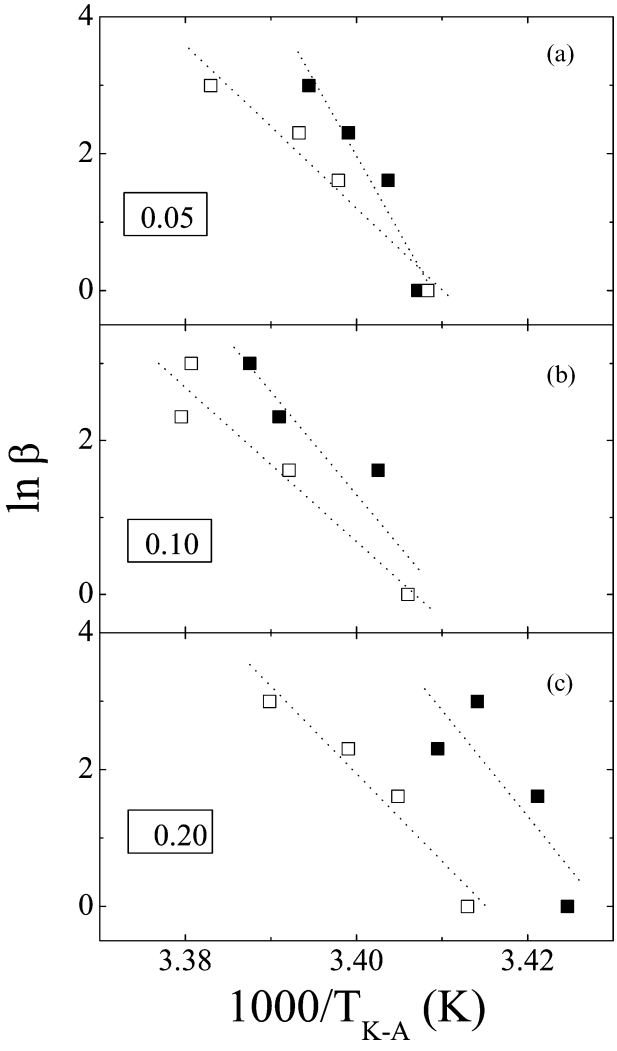

Figure 8. Arrhenius behaviour for the *K*–Sm*A* or melting transition: lnβ (K min^{-1}) versus 1/*T* (K) for various densities: (A) 0.05 g cm^{-3}; (B) 0.10 g cm^{-3}; (C) 0.20 g cm^{-3}. Dotted lines are the fits to the data points. Closed and open symbols represent the aligned and unaligned systems, respectively.

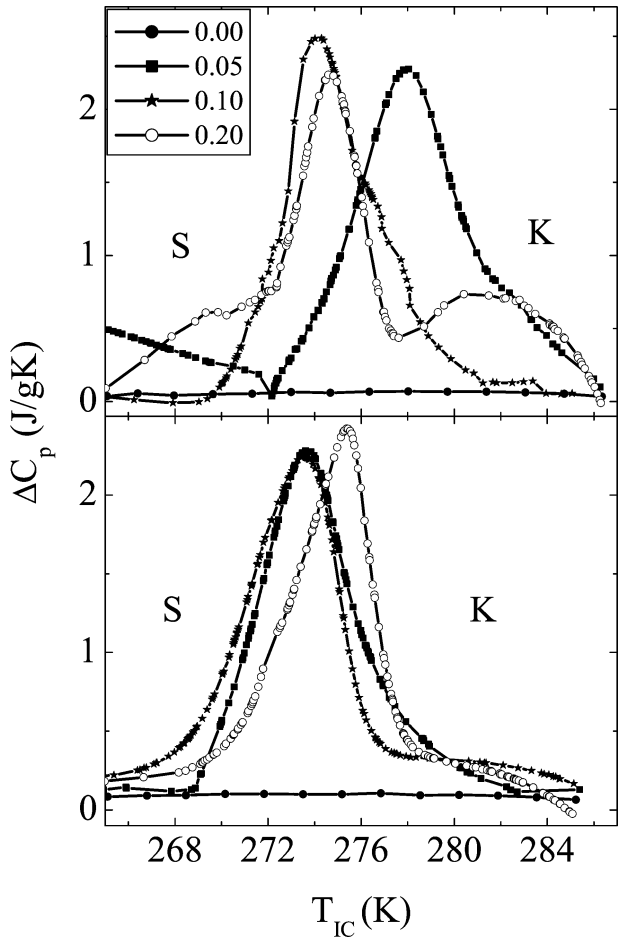

Figure 9. Effect of aerosil density on alignment: density-dependent heating scan at 5 K min^{-1} ramp rate for IC transition plotted as the excess of specific heat capacity (*J*/*g*) versus temperature (*K*) plot for all densities of aerosils. Upper section: Aligned, Lower section: Unaligned systems, respectively.

represents that the crystal grows as the density of aerosil nanoparticles increases in the aligned system from 0.05 to 0.20 g cm^{-3}, as shown in Figure 10. The melting peak becomes smaller and shows a decrease in its enthalpy as the density of nanocolloids increases in the aligned system, as shown in Figure 11.

The variation in peak position in the IC transition increases and the temperature range between IC and melting transitions (denoted by R_{IC} in Kelvin) decreases. For the melting transition, the variation

Table 1. Data details for IC and melting transitions (*K*–Sm*A*) for aligned and unaligned systems: the type of system, density of aerosil particles ρ (g cm^{-3}), transition temperature *T* (K), enthalpy ΔH (KJ mol^{-1}), activation energy ΔE (KJ mol^{-1}) and temperature range ΔR (K) for IC and melting transitions where the subscripts IC and KA are used for the IC and melting transitions, respectively.

System	ρ	T_{IC}	T_{KA}	ΔH_{IC}	ΔH_{KA}	ΔE_{IC}	ΔE_{KA}	ΔR_{IC}	ΔR_{KA}
Aligned	0.05	277.9	293.6	3.92	18.20	0.14	1.84	15.7	11.2
Aligned	0.10	274.1	293.8	3.96	37.50	0.21	1.28	19.7	11.1
Aligned	0.20	275.7	292.3	4.25	17.37	0.18	1.45	17.5	12.4
Unaligned	0.05	273.8	294.3	3.79	52.90	0.34	0.99	20.4	10.8
Unaligned	0.10	272.6	295.0	3.94	58.30	0.26	0.88	21.6	10.6
Unaligned	0.20	275.4	293.3	4.09	55.96	0.19	1.06	17.7	12.0

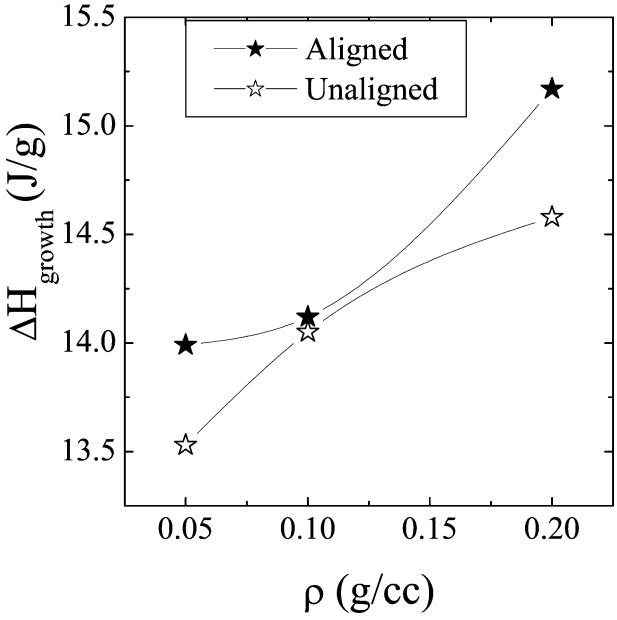

Figure 10. Effect crystal growth on alignment: Crystal growth versus aerosil density for aligned and unaligned samples. Closed and open symbols represent the aligned and unaligned systems, respectively.

in peak position decreases and the temperature range between the melting and smectic A transitions (denoted by R_{KA} in Kelvin) increases. These data are given in Table 1.

3.4. *Change in the percentage crystallinity*

The change in percentage crystallinity can be seen in the system using the following equation. To know how much of the system is crystalline, the latent heat for IC and melting transitions were calculated, and were used to calculate percentage crystallinity of the system.

$$\Delta H' = \Delta H_m - \Delta H_c, \tag{4}$$

$$\Delta\%\text{Crystallinity} = \frac{\Delta H'}{\Delta H_m^* * m_{total}} \times 100, \tag{5}$$

where ΔH_m and ΔH_c are the latent heat of melting and IC transitions, respectively, ΔH_m^* is the specific heat of melting, and m_{total} is the total mass of the sample used. Figure 12 shows the change in percentage crystallinity of the aligned system as a function of aerosil density after subtracting the percentage crystallinity of aligned IC transition from the unaligned IC transition. This figure shows that the aligned system is 14% more crystalline than the unaligned system at $0.05\,g\,cm^{-3}$, and then crystallinity increases up to 15% for the highest density of

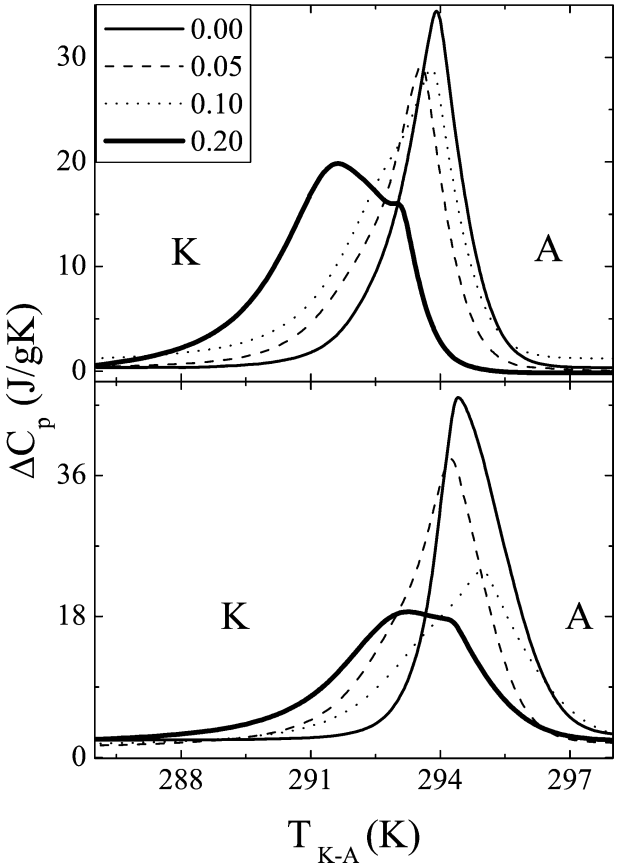

Figure 11. Blow up of the *K*–Sm*A* transition for all densities at $5\,K\,min^{-1}$ heating ramp rate plotted as the excess of specific heat capacity ($J\,g^{-1}\,K^{-1}$) versus temperature plot (K). The upper section shows aligned systems and the lower section shows unaligned systems.

aerosil $0.20\,g\,cm^{-3}$. Hence, the aligned system shows an increase in its percentage crystallinity as it moves from a solid state (*S*) to crystalline state (*K*) through IC transition and shows a growth in induced crystallisation as shown in Figure 10.

4. Discussion and conclusions

4.1. *Activated kinetics of aligned nanocolloids*

IC and melting transitions show an interesting change in their thermodynamics following Arrhenius behaviour under the effect of alignment. This type of study can further be used in several applications to manufacture electronic devices where LCs and their mixtures are used to activate and deactivate transitions for displays, for example, in LCD screens. In the aligned system, IC and melting transitions show changes in their peak positions, peak shapes, temperature ranges, enthalpy and their activation energy. These results can be explained in terms of molecular and surface interaction between LC molecules and aerosil particles, and occurred stiffness in the aligned system.

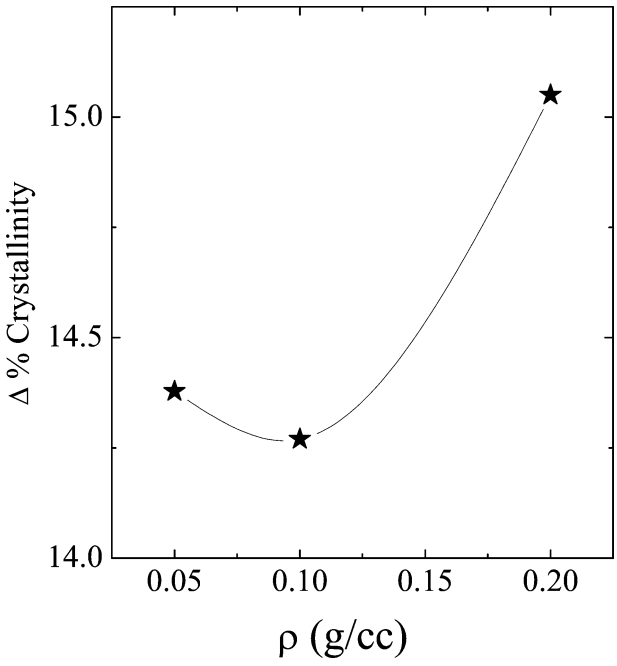

Figure 12. Change in percentage crystallinity versus aerosil density plot for the aligned IC transition.

The aerosil nanoparticle SiO_2 (silica) spheres are coated with hydroxyl (–OH) groups exposed on the surface. The hydroxyl groups on the surface enable the spheres to hydrogen bond and form a thixotropic, fractal gel in an 8CB organic medium. The hydrophilic nature of the aerosils allows the silica particles to weakly hydrogen bond to each other and form a gel in an organic solvent. Due to the formation of a weak hydrogen bond between LC and aerosil particles, an interaction between 8CB and aerosil nanoparticles takes place (*4, 20*). In the presence of alignment, the 8CB LC molecules become aligned and form aligned domains. In the presence of alignment, the aligned domains of LC molecules impose a force on nanocolloids and hence aerosil nanoparticles also become aligned in the direction of the aligned domain of LC molecules. Hence, due to the alignment created in the nanocolloidal system, the system produces a strain between aerosil nanoparticles. Due to the increase in molecular alignment, the aligned system shifts towards higher energy, and the IC transition shows a shift towards higher temperature as well as an increase in its crystallization in terms of enthalpy (or growth). Whereas melting transition is an endothermic transition (as IC shows an exothermic peak), it shows changes in peak position and its enthalpy in the opposite way, and hence shows a decrease in its enthalpy with shifting transition towards lower temperature in the aligned system. Since IC and melting transitions show opposite changes in the aligned system, hence the temperature range between IC and melting shows an decrease whereas the temperature range between melting and smectic *A* shows an increase in the temperature range.

The thermodynamics of the transitions reveal a relationship between their enthalpy and their activation energy. Figures 13 and 14 show comparative plots between the enthalpy and activation energy of the aligned system for IC and melting transitions, respectively. These figures indicate that enthalpy and activation energy of the transitions follow a pattern of variation but in opposite directions. The enthalpy of IC transition increases as the nanocolloidal density increases in the aligned system, and its respective activation energy decreases following the same pattern of variation. On the other hand, the enthalpy of melting transition decreases as nanocolloidal increases in the aligned system and its associated activation energy increases. Since the aligned system moves towards higher energy level due to the increased molecular alignment, the IC transition shows more crystallization in terms of an

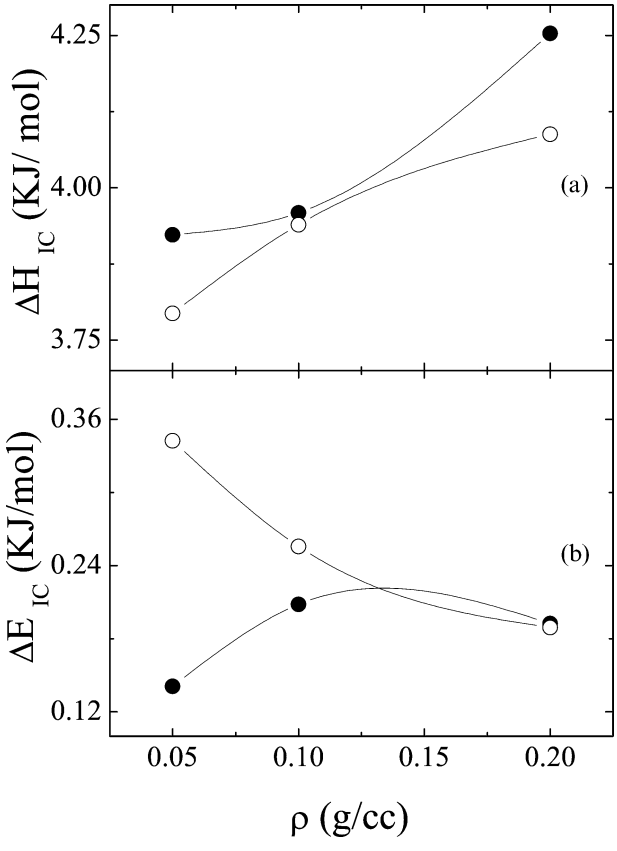

Figure 13. Activated kinetics of the IC transition. (A) Change in enthalpy ($KJ\,mol^{-1}$) versus density for aligned and unaligned systems. (B) Change in activation energy ($KJ\,mol^{-1}$) versus aerosol density plot for aligned and unaligned systems. Closed and open symbols represent the aligned and unaligned systems, respectively.

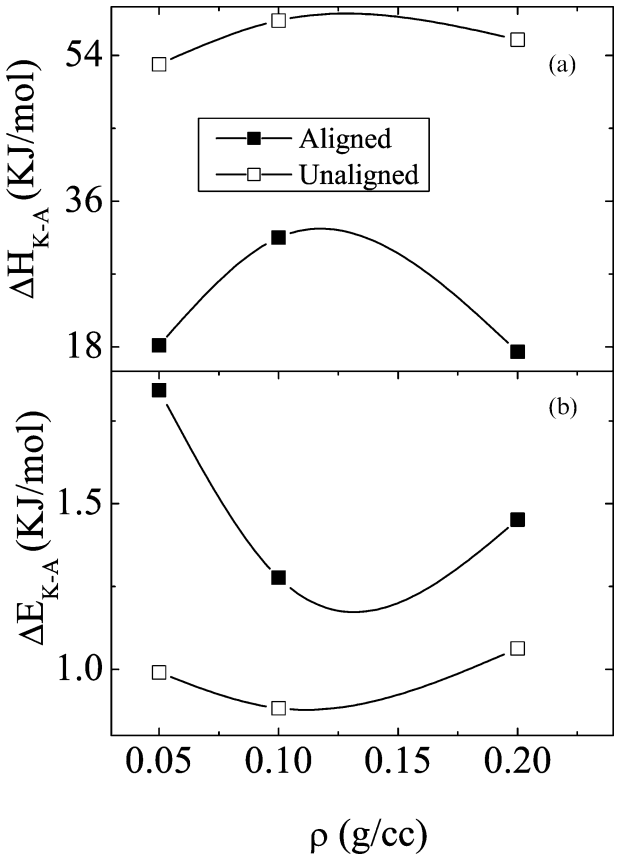

Figure 14. Activated kinetics of the melting transition (*K*–Sm*A*). (A) Change in enthalpy ($KJ\,mol^{-1}$) versus density for aligned and unaligned systems. (B) Change in activation energy ($KJ\,mol^{-1}$) versus aerosil density plot for both aligned and unaligned systems. Closed and open symbols represent the aligned and unaligned systems, respectively.

exothermic peak and releases more energy and shows an increased enthalpy and hence needs less activation energy for the transition in the aligned system. On the other hand, the melting transition absorbs energy (as it is a endothermic peak) shows a decrease in its enthalpy and hence needs more activation energy. The variation pattern of enthalpy and activation energy as a function of nanocolloidal density depends on the stiffness and strain occurring in the gel due to the alignment effect and interaction between aerosil nanocolloids and LC molecules. Under the effect of alignment, LC becomes more aligned and the gel may become stiffer. For the lowest density of nanocolloids $0.05\,g\,cm^{-3}$, in the aligned system, the gel becomes stiffer due to the interaction between LC molecules and aerosil nanoparticles under the effect of magnetic force. As nanocolloidal density increases in the aligned system, the rate of interaction increases and makes the gel stiffer and shows an increase in the enthalpy of IC and decrease in the melting transition.

The data for the aligned and unaligned systems are given in the Table 1.

4.2. *Conclusions*

Aligned nanocolloids in 8CB dispersions bring interesting changes in the thermodynamics of the aligned system and show the activated kinetics of IC and melting transitions following an Arrhenius behaviour. Heating scans were performed using DSC for aligned and unaligned systems. In the aligned system, IC transition shifts significantly towards a higher temperature with an increase in its peak shape and size, whereas the melting transition shifts towards a lower temperature with decreasing enthalpy. In addition, rate-dependent heating scans of the aligned system show an increased temperature shift for IC transition and decreased temperature shift for melting transition following an Arrhenius behaviour towards a lower temperature as the ramp rate decreases. As the density of nanocolloids increases in the aligned system, the system becomes more crystalline and shows growth in IC. Furthermore, with the increase in the nanocolloids in the aligned system, the enthalpy of the IC transitions increases and its associated activation energy decreases whereas the melting transition shows an decrease in its enthalpy and increase in activation energy. This behaviour of the aligned system can be explained in terms of change in alignment, surface interaction between aerosil nanoparticles and LC molecules, and the changes in the character and stiffness of the nanocolloidal gel in aligned 8CB+silica.

As nanocolloidal particles are added to bulk 8CB, a molecular disorder takes place and shows the surface interaction between molecules where aerosil nanoparticles are found to be coated with 8CB molecules and interact with each other under a weak hydrogen bond interaction (*20*). In the presence of alignment, the 8CB molecules become more aligned and ordered under the force of the magnetic field and this makes the system more crystalline. The increased alignment in the LC and mutual interaction between aerosil nanoparticles and LC molecules make the gel stiffer. Hence, the aligned system releases more energy in terms of exothermic (IC) transitions and shows an increase in its enthalpy and needs less activation energy. On the other hand, the melting transition is an endothermic transition, hence shows an decrease in its enthalpy and needs more activation energy in the aligned system.

Acknowledgements

The author is grateful to Germano Iannacchione for many useful discussions and to J. C. MacDonald for help with the DSC instrument.

References

(1) Bellini T.; Radzihovsky L.; Toner J.; Clark N.A. *Science* **2001**, *294*, 1074–1079.
(2) Bellini T.; Clark N.A.; Degiorgio V.; Mantegazza F.; Natale G. *Phys. Rev. E* **1998**, *57*, 2996–3006.
(3) Jin T.; Finotello D. *Phys. Rev. Lett.* **2001**, *86*, 818–821.
(4) Iannacchione G.S.; Garland C.W.; Mang J.T.; Rieker T.P. *Phys. Rev. E* **1998**, *58*, 5966–5981.
(5) Sharma D.; Iannacchione G.S. *J. Phys. Chem. B* **2007**, *111*, 1916–1922.
(6) Leheny R.L.; Park S.; Birgeneau J.L.; Gallani J.L.; Garland C.W.; Iannacchione G.S. *Phys. Rev. E* **2003**, *67*, 011708–011720.
(7) Bagmet A.D.; Tsykalo A.L. *J. Eng. Phys.* **1987**, *52*, 279–285.
(8) Li F.; Doane W.J.; Kli A.J. *Japan. J. Appl. Phys.* **2006**, *45*, 1714–1718.
(9) de Gennes P.G.; Prost J. *The Physics of Liquid Crystals*, 2nd edn; Clarendon Press: Oxford, 1993.
(10) Lizuka E. *Int. J. Polymeric Mater.* **2000**, *45*, 191–238.
(11) Liang D.; Borthwick M.A.; Leheny R.L. *J. Phys.: Condens. Matter* **2004**, *16*, S1989–S2002.
(12) Sharma D.; Shukla R.; Singh A.; Nagpal A.; Kumar A. *Adv. Mater. Opt. Electron.* **2000**, *10*, 251–259.
(13) Ernst C.R.; Schneider G.M.; Rflinger A.W.; Weißflog W. Ber. Bunsenges. Phys. Chem. **1998**, *102*, 1870–1873.
(14) Donth E.; Korus J.; Hempel E.; Beiner M. *Thermochimica Acta* **1997**, *305*, 239–249.
(15) Sharma D.; Iannacchione G.S. *J. Chem. Phys.* **2007**, *126*, 094503–094508.
(16) Sharma D.; MacDonald J.C.; Iannacchione G.S. *J. Phys. Chem. B* **2006**, *110*, 16679–16684.
(17) Sharma D.; Shukla R.; Kumar A. *Thin Solid Films* **1999**, *357*, 214–217.
(18) Mehta N.; Sharma D.; Kumar A. *Physica B* **2007**, *391*, 108–112.
(19) Sharma D.; Dwivedi S.K.; Shukla R.K.; Kumar A. *Mater. Manufact. Process.* **2003**, *18*, 93–104.
(20) Sharma D.; MacDonald J.C.; Iannacchione G.S. *J. Phys. Chem. B* **2006**, *110*, 26160–26169.
(21) Clegg P.S.; Stock C.; Birgeneau R.J.; Garland C.W.; Roshi A.; Iannacchione G.S. *Phys. Rev. E* **2003**, *67*, 021703–021715.
(22) Clegg P.S.; Birgeneau R.J.; Park S.; Garland C.W.; Iannacchione G.S.; Neubert M.E. *Phys. Rev. E* **2003**, *68*, 031706–031712.
(23) Vogel H. *Phys. Z.* **1921**, *22*, 645–646.
(24) Fulcher G.S. *J. Am. Ceram. Soc.* **1925**, *8*(6), 339–355.
(25) Maximean D.; Rosu C.; Yamamoto T.; Yokoyama H. *Mol. Cryst. Liq. Cryst.* **2004**, *417*, 215–226.
(26) Blum F.; Padmanabhan A.; Mohebbi R. *Langmuir* **1985**, *1*, 127–131.